JAST, Vol. 3, No. 1, pp 1–15

JAST
Journal of Aerospace Science and Technology

Experimental Study of Vortex Shapes behind a Wing Equipped with Different Winglets

M. Nazarinia[1], M. R. Soltani[2], K. Ghorbanian[3]

An extensive experimental study is conducted to examine the effects of different winglet-shapes and orientations on the vortex behind a wing, static surface pressure over the wing, and wake of a swept wing at various angles of attack. Four types of winglets, spiroid (forward and aft), blended, and winggrid are used in this investigation. Wing static surface pressure measurements are obtained for both chordwise and spanwise as well as the wake profiles at various angles of attack using the aforementioned winglets. The data are compared with those without winglet – that is, bare wing. The results show that integration of winglets change the flowfield over and around the wing significantly. Further, it is found that certain winglet configurations improve both the wake and the wing pressure distribution. The total pressure in the wake of the model varies drastically when the wing is equipped with winglets.

NOMENCLATURE

b	wing span (m)
$C_P = \frac{2(P-P_\infty)}{\rho_\infty U_\infty^2}$	static pressure coefficient
$C_{PT} = \frac{2(P_T-P_\infty)}{\rho_\infty U_\infty^2}$	total pressure coefficient
P	static pressure (N/m^2)
P_T	total pressure (N/m^2)
P	ambient pressure (N/m^2)
Re	Reynolds number based on free stream conditions and airfoil chord
x	airfoil abscissa
y	airfoil ordinate
x/c	airfoil coordinate (non-dimensional)
u	x-component (axial) velocity (m/s)
U	freestream velocity (m/s)
$z = 0$	at the center of the test section (m)
α	angle of attack (degrees)
Λ_{LE}	sweep angle (degrees)
$\eta = \frac{2y}{b}$	non-dimensional span
ρ_∞	ambient density (kg/m^3)
$\zeta = \frac{2z}{b}$	non-dimensional height above the wing surface

1. *Senior Research Engineer, Dept. of Aerospace Eng., Sharif Univ. of Tech., Tehran, Iran, Email: mehdi_nazarinia@yahoo.com.*
2. *Associate Professor, Dept. of Aerospace Eng., Sharif Univ. of Tech., Tehran, Iran.*
3. *Associate Professor, Dept. of Aerospace Eng., Sharif Univ. of Tech., Tehran, Iran.*

INTRODUCTION

Aerodynamic improvements of aircraft through modification of flow in the wingtip region have been the focus of many years of research and study. For an aircraft in cruise flight, drag is balanced by the engine thrust which directly sets the fuel consumption. Hence, drag reduction will lead to fuel savings and then to a lower operating cost. As a result, designers have been searching for methods and technologies to reduce the required fuel consumption of commercial aircraft for many years. Numerous investigations using passive devices, such as tailored wingtips, endplates, winglets, and tip sails have been conducted. The fundamental premise of these fixed geometry concepts is to reduce the induced drag and thereby minimize the trailing vortex strength. Induced drag is responsible for 30-40% of the total drag of a transport-aircraft in cruise condition, and downgrades the climb performance considerably. Increasing the effective aspect ratio with devices such as endplates and winglets does occur

although this is partially offset by the increase in viscous drag from the added wing wetted area [1-2]. Well-designed winglets, which direct a component of the lift into the thrust direction and tip sails, have indicated the potential for induced drag reductions [3].

As noted by Whitcomb [4], Lanchester applied for a patent on wing end plates in 1897. A steady stream of publications and patents dealing with various concepts for induced drag reduction has appeared since then. From theoretical studies of wings with end plates, done as early as 1924 [5-7], to computational studies performed in the 1960s and 1970s as vortex lattice methods became more accessible, and to recent system studies, drag reduction devices, especially wing tip devices, have remained popular topics in the aerodynamic literature [8].

The winglet concept; however, remained immature until Richard Whitcomb of the Langley Research Center investigated its aerodynamic advantages on a transport aircraft in the 1970s. The winglet, developed by Whitcomb, was tested on a KC-135A tanker loaned to NASA by the Air Force. The flight test showed that winglets could increase the aircraft's range by as much as seven percent at cruise speeds. The first application of NASA's winglet technology in industry was on General Aviation business jets. In recent years, many modification kits have been offered for installing winglets on aviation aircraft that originally did not have such devices. Further, a NASA contract in the 1980s [9] assessed winglets and other drag-reduction schemes. The results indicated that wingtip devices (winglets, feathers, sails, etc.), if designed as an integral part of the wing, can improve drag-due-to-lift efficiency by as much as 15%.

A close look at the drag breakdown of a typical civil transport aircraft (Figure 1), reveals that the skin friction and lift induced drag together represent more than 80% of the total drag and may offer the highest potential for drag reduction while the remaining components represent only about 20% of the total drag. Induced drag is one of the major contributors (about 35%) of the total aircraft drag. Various research programs have concentrated on using wing tip devices to increase the effective span of the wing. Integrated winglet concepts with continuous evolution of the wing tip shape have been studied by several research centers worldwide. Among the various types studied, new concepts such as spiroid winglets, focus of the present work, seem to be the most promising ones [10].

Studies employing active devices have also been undertaken to try to reduce the drag at a given lift by insertion of tip turbines, propellers, and air jets into the vortex region [11-13] (Figure 2). However, tip turbines are found to yield the largest drag reduction. The tip propellers are reported to displace the vortices further outboard, increasing the effective aspect ratio.

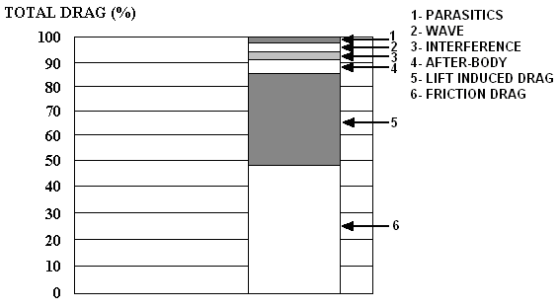

Figure 1. Drag breakdown of a typical transport aircraft [10].

Improvements are also found from the blowing jets but the extra weight and complexity of these devices have precluded their use on aircrafts.

Recent work by Eppler [14] has suggested that a local small dihedral in the tip region of a wing may be an effective mean to reduce its drag through the nonlinear effect of induced drag for a given lift. Several interesting results are concluded from Eppler's study. First, a wingtip with a dihedral of about 10° has a lower induced drag than a planar wing with the same length; i.e. smaller span. Second, positive dihedral induces a negative lift on the wake and therefore a positive lift on the wing. Negative dihedral indicates the opposite and thus a wing with a downward pointing tip performs poorer. However, experimental studies to verify the above theoretical works have not been extensive.

As mentioned earlier, there are numerous experimental and numerical investigations regarding different types of wingtip devices. There are even many flight test reports on a few types of winglets especially suit-

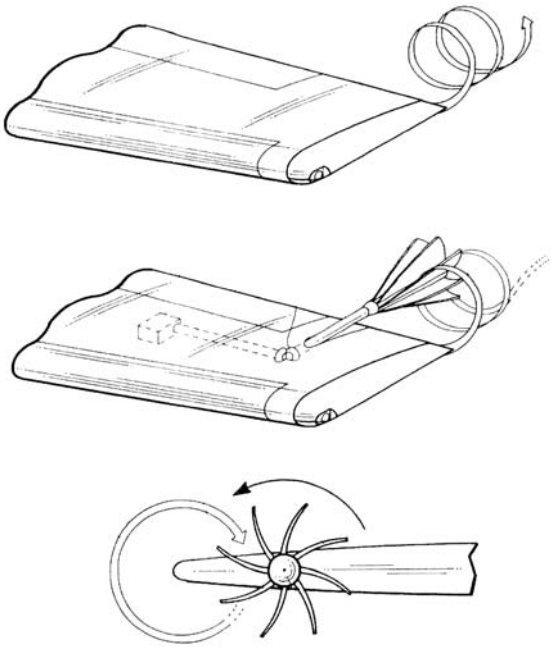

Figure 2. Schematic of a wingtip turbine [11].

able for sailplanes. Fore more information, the reader is referred to references [15-26] for a selective range of numerical and experimental investigations. Several characteristics of endplates in terms of optimization of the design are currently under investigation. Reference [25] has revealed a short description on a special kind of winglet, spiroid winglet. In addition, researchers at ONERA have carried out some numerical calculations on spiroids and blended winglets as well. Nonetheless, to the authors' knowledge, experimental studies in this field are rare and there is a need for further investigation.

The main goal of this work is to study the effects of various winglet shapes on the wing surface pressure distribution as well as the wake profile. A basic study of the flowfield surrounding the winglets and wing was performed with simple models to guide the selection of winglet configurations. Optimum shape of winglets, location and spacing, their angles of attack, dihedral, and sweep were the unknowns to be determined. It is hoped that this work along with other studies will further reduce the existing gap between the experimental and theoretical knowledge of the effects of winglets on the flowfield over and behind the wing.

EXPERIMENTAL APPARATUS

All experiments were conducted in the low speed wind tunnel of the Department of Mechanical Engineering at Sharif University of Technology. The wind tunnel is an open circuit indraft tunnel with a rectangular test section of 45 cm × 45 cm × 160 cm. The maximum obtainable speed in the test section of this tunnel is approximately 45 m/sec. A half-span wing with sweep angle of 20 degrees is mounted in the test section. The angle of attack could be varied manually from zero to 90 degrees. Figure 3 shows the tunnel and the model as well as different winglet shapes used in this investigation.

As a first step, the flow quality of the wind tunnel is investigated using a hot-wire anemometry system. The variation of the turbulence intensity with velocity is shown in Figure 4 [27, 28]. It can be seen that the turbulence intensity decreases as the wind tunnel speed is increased. Therefore, for velocities higher than 10 m/s, the turbulence intensity is low; hence, making the tunnel suitable for these kinds of research.

Four types of winglet shapes, spiroid [29] (forward and aft), blended [31], and winggrid [32, 33] are used in this investigation (Figure 5). The wing model used in this study has an average chord of 15.7 cm and is constructed with fiberglass skins formed in molds that are manufactured using a numerically controlled milling machine. The Spiroid-typed winglets are constructed with aluminum and the remaining ones with plexi-glass. The wing model is equipped with 26 and

(a)

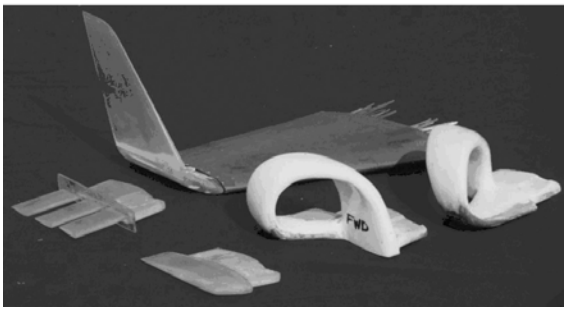

(b)

Figure 3. (a) Wind tunnel and (b) the model including winglet shapes, (not to scale).

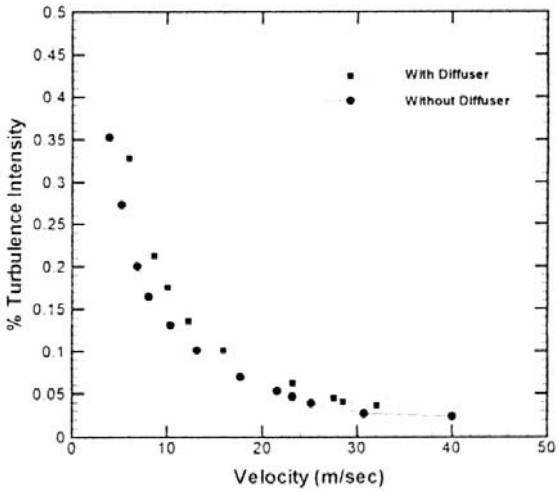

Figure 4. Diffuser effect on tunnel turbulence intensity [27,28].

25 pressure ports on the upper and lower surface, respectively, where 11 of them are along its span.

Due to the small thickness of the wing, pressure ports on the upper and lower surfaces could only be embedded in one location. Spanwise and chordwise positions of the pressure ports are shown in Figure 6. While the chordwise port locations are on the

maximum thickness of the airfoil, the spanwise port locations are at $\eta = \frac{2y}{b} = 0.654$.

A 32-tube rake probe is mounted horizontally from the back of the model. A traversing mechanism incrementally positions the probe across the wake. The probe is positioned at the tunnel centerline and the wake survey data are measured at a single traverse plane (at a distance of 2.0 times average wing chord) downstream of the model trailing edge (Figure 7). Both surface pressures and wake data are obtained using very accurate pressure transducers. Each transducer data is collected via a multiplexer and transferred to the computer through a 16-bit Analogue-to-Digital (A/D) board. Various sampling rates are performed and finally the best one is selected. Each data point shown here are ensemble averages of several hundred data points taken several times in different days. This was done to ensure data repeatability and accuracy since the authors were not able to find similar data for comparison.

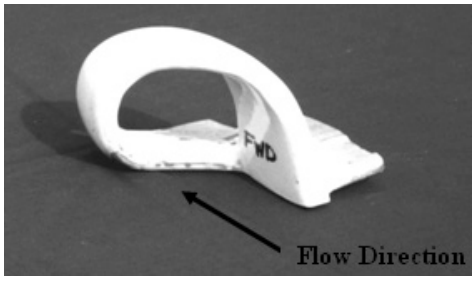

(a) FWD spiroid

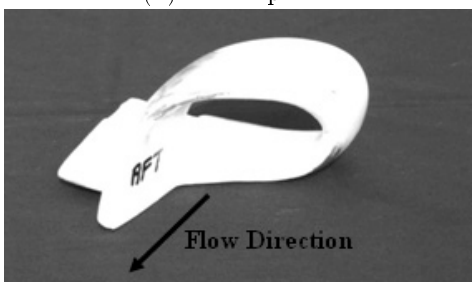

(b) AFT spiroid

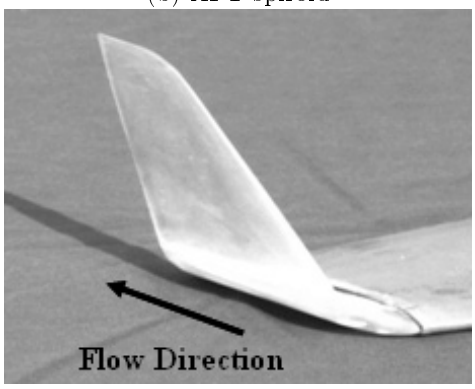

(c) Blended winglet

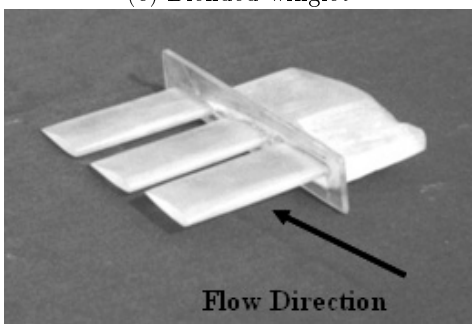

(d) Wing grid

Figure 5. Winglet models.

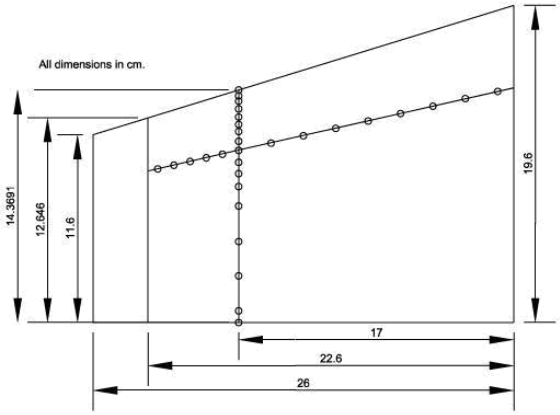

Figure 6. Chordwise and spanwise cross section of the wing for all investigated cases.

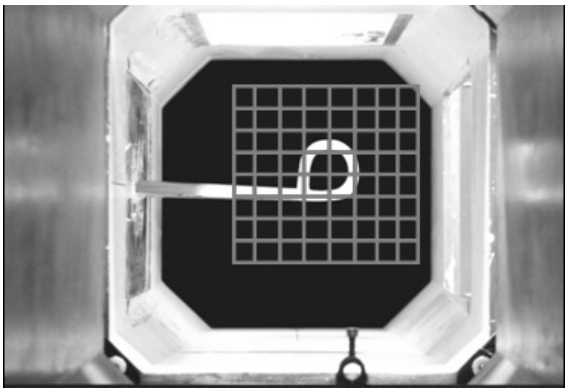

Figure 7. Domain of total pressure measurements behind the wing and winglet model mounted in the middle of test section.

RESULTS AND DISCUSSIONS

All measurements presented in this paper are conducted at a Reynolds number of 0.2×10^6, using four different types of winglet at various angles of attack. Static surface pressure data, both chordwise and spanwise as well as the wake data for all winglets are measured. Each data set acquired in these tests comprised of approximately 2500 points. Reduction of the raw pressure data yielded an axial velocity component as well as static and total pressure coefficients. For

reliability purposes, data is acquired over a series of wind tunnel tests conducted at different times. The repeatability of the pressure data from the winglet models is also analyzed.

Flow Visualization

In order to recognize the wing flow pattern, tufts are attached over the wing surface. Figure 8 shows the flow field over the wing for different winglet shapes photographed at 10 degrees angle of attack. The flow direction over a typical swept and tapered wing on the upper surface is from tip to root which is exactly the same as its stall pattern (Figure 9). The flow pattern over the model used in this investigation follows the same manner. The stall characteristic is assumed to be similar to those for the wing without winglet (Figure 8). However, in cases including winglet, the flow field is changed drastically; thus, changing the stall characteristics. It should be mentioned that different winglets have resulted in different flow fields.

It is seen that for α=10°, the flow is partially separated, especially near the TE region. The positions where the flow field is separated are totally different for each winglet. For the bare wing and wing grid, the solution is to some level similar. The flow behaves as fully separated at the wingtip in TE. This separation is more evident for the wing grid.

The results obtained for the flow field of the spiroid winglet shows the most differing characteristics. The direction of the flow for spiroid winglets, both FWD and AFT, is from root to tip, which is in contrast to what is expected – that is, from tip to root. This type of movement actually makes the effective wing aspect ratio larger than the actual wing.

Figures 8c-d shows the flow direction over FWD and AFT spiroid winglets, respectively. Figure 8c shows that for the FWD spiroid winglet at α=10° the wingtip vortex is mixed with the vortex exerted from the upper surface of the wing so that the mere wingtip vortex does not exist any longer; however, the opposite is true for the AFT spiroid winglet one. Referring to Figure 8d, the two separate vortices, the wingtip and the upper surface vortices are clearly seen. By observing the tufts installed at the TE of the wing in Figure 8e, the wing grid case, one may say that the flow is totally separated. Figure 18e shows this separation as well.

Static Surface Pressure Distribution

Figures 10 and 11 show both chord wise and span wise static pressure distributions for the bare model at various angles of attack. Data shown in Figure 10 is similar to that of the 2-D data where the magnitude of C_P increases with increase in the angle of attack, creating more lifts. It should be noted that since the model is very thin, it was very challenging to embed pressure taps near the trailing edge; hence, all chordwise surface pressure data are for x/c≤0.7. The spanwise static pressure data, Figure 11, indicates that C_P is almost constant along the wing span for both upper and lower surfaces at low angles of attack but their values are different. However, at 10 degrees angle

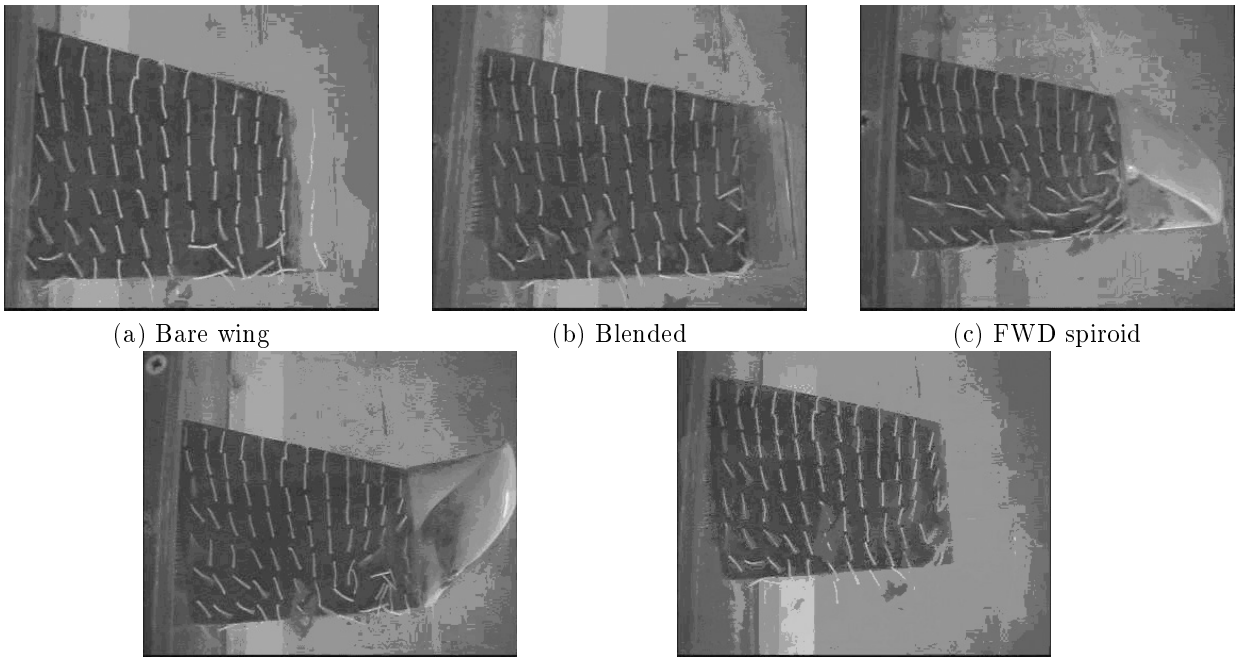

(a) Bare wing (b) Blended (c) FWD spiroid

(d) AFT spiroid (e) Wing grid

Figure 8. Flow visualization with tufts, $\alpha = 10^{\circ}$

of attack, C_P distribution over the wing upper surface differs significantly from that of the 5 degrees one. The spanwise pressure distribution for α=10° shows the existence of an area of low pressure from the midspan, η=0.4 to $\eta\approx$0.8, a vortex like flow. This is probably due to the wing sweep angle [10, 16]. As mentioned in references [34-35], for a swept wing at moderate to high angles of attack, a low-pressure area similar to that of Figure 11 will exist over the wing surface.

Figures 12 and 13 show the effects of spiroid winglets, FWD and AFT, on pressure distribution , both chord-wise and span-wise, at two different angles of attack. The pressure data for the bare wing is also shown for comparison. From these figures, it is clearly seen that the spiroid winglet changes both chordwise and spanwise surface pressure distributions. This is especially true for the upper surface pressure data. For the AFT spiroid one, it is seen that the spanwise pressure distribution near the wingtip is lower than that of the FWD spiroid one, indicating again the existence of a weaker wingtip vortex for the AFT spiroid case, Figure 13.

The effects of blended winglet on the wing surface pressure distribution, chordwise and spanwise, at 10 degrees angle of attack are shown in Figure 14. The surface pressure distribution for the bare wing at the same angle of attack is also provided for comparison. It can be seen that the blended winglet has changed both spanwise and chordwise pressure distributions for the wing upper surface while its effect on the lower surface is minimal. Figure 14a indicates that the blended winglet has a pronounced effect on the wing pressure recovery region, x/c>0.2. Also it has some effects on the leading edge pressure distribution even if not significant. Here, one may conclude that this winglet has slightly increased the laminar flow region in the vicinity of the leading edge. Figure 15 shows static surface pressure distribution, chordwise and spanwise, over the model equipped with the winggrid. The results illustrate that the winggrid does not have a significant impact on the wing surface static pressure distribution, both spanwise and chordwise. Nevertheless, slight modifications in the static pressure near the wing leading edge are observed. Further, Figure 15a shows that the winggrid reduces the total wing lift slightly in comparison to the bare wing at the same angle of attack.

Static Surface Pressure Distribution with Turbulator Tape

The high Reynolds number test condition corresponds to a typical flight state. To anchor our data obtained in the wind tunnel, the wing with winglets are tested at a matching low Reynolds number condition with the boundary-layer tripping (forced transition) strategy used in a conventional wind tunnel. Boundary-layer transition strip (turbulator tape) is placed only on the upper surface of the wing. The strip consists of a band (0.5 cm wide) of sandpaper grains set in a

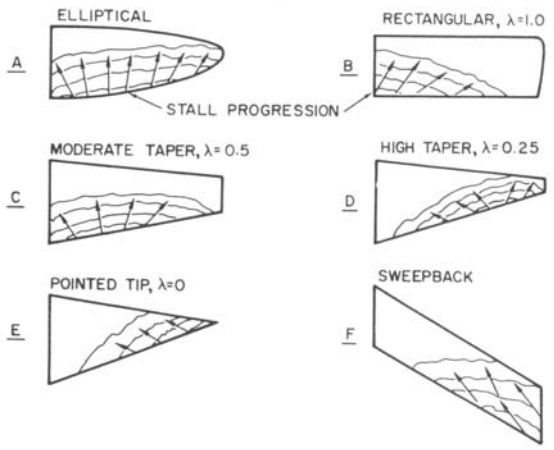

Figure 9. Stall patterns over several wing shapes [34].

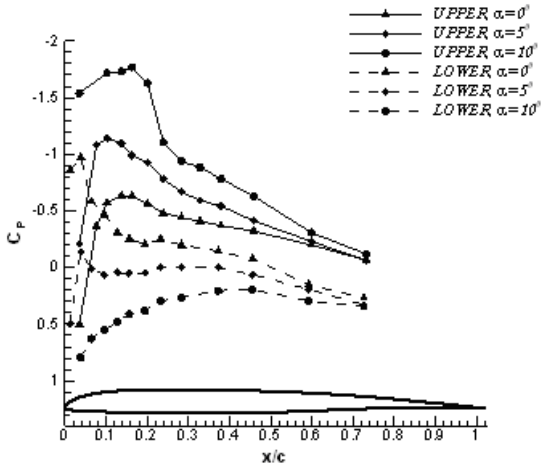

Figure 10. Chordwise surface static pressure distribution over the bare model, η = 0.654.

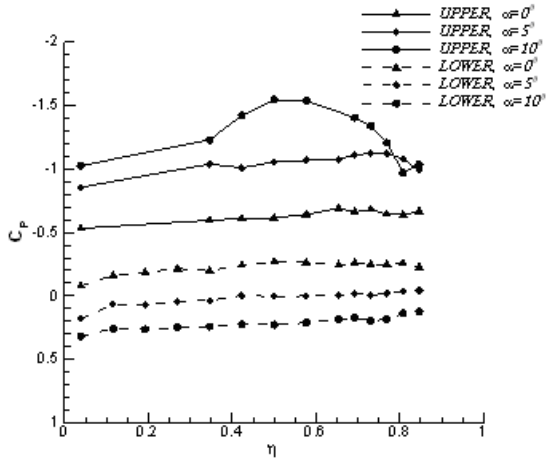

Figure 11. Spanwise surface static pressure distribution over the bare model, x/c≈0.7.

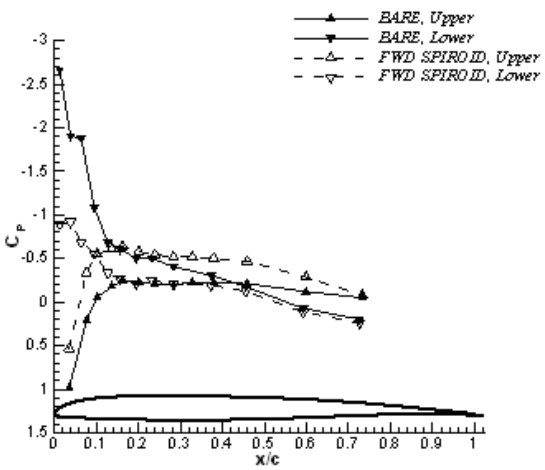

(a) $\alpha = 5°$, FWD spiroid

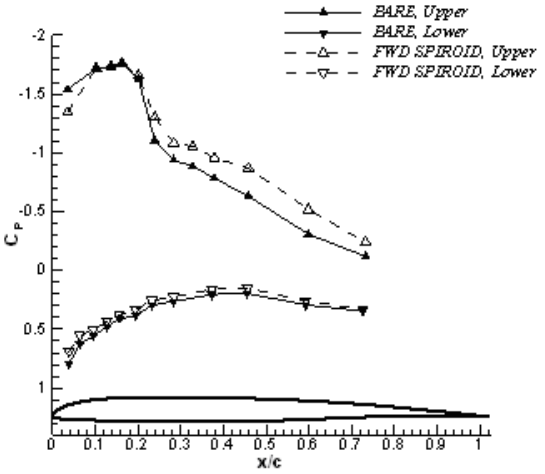

(b) $\alpha = 10°$, FWD spiroid

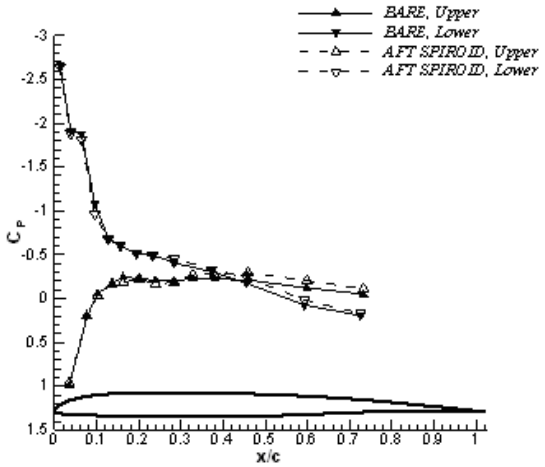

(c) $\alpha = 5°$, AFT spiroid

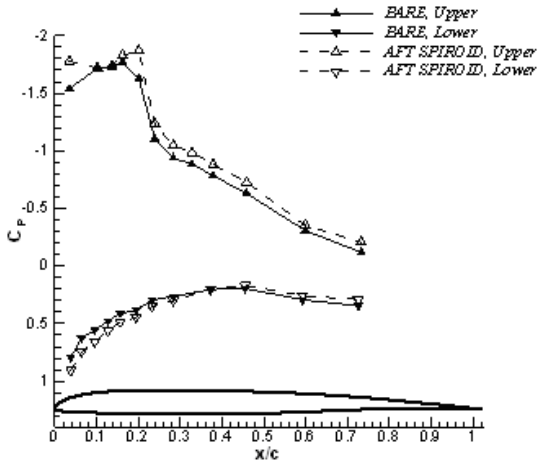

(d) $\alpha = 10°$, AFT spiroid

Figure 12. Effect of spiroid winglet on the chordwise static pressure distribution.

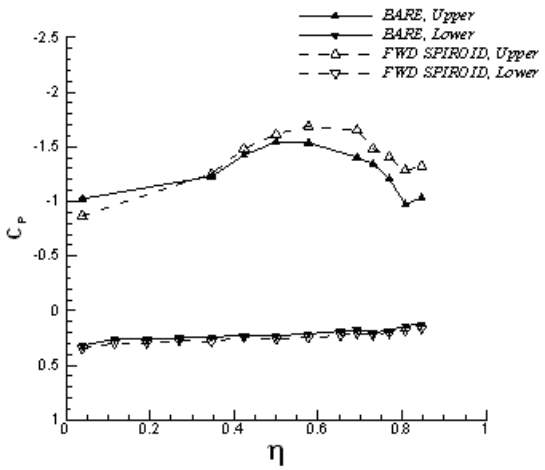

(a) FWD spiroid

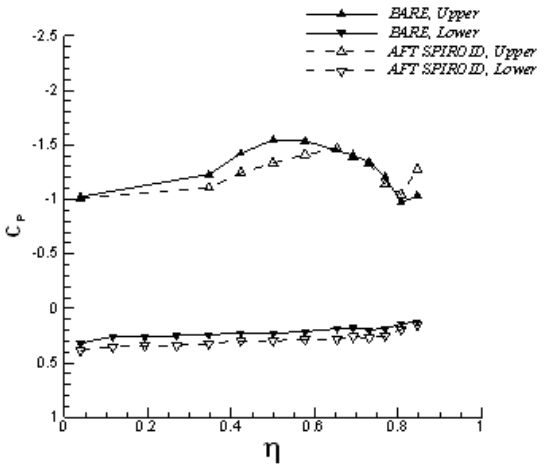

(b) AFT spiroid

Figure 13. Effect of spiroid winglet on the spanwise static pressure distribution, $\alpha = 10°$.

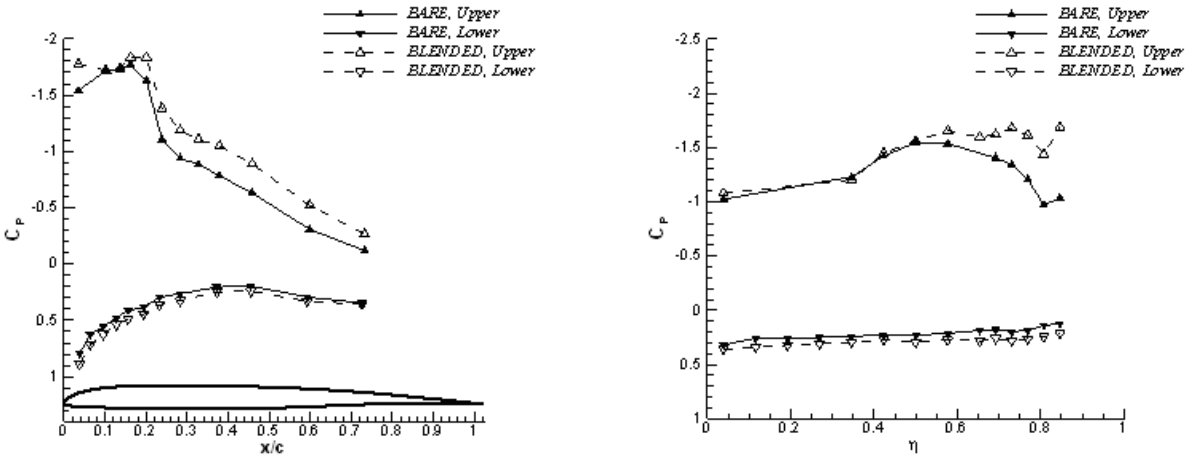

(a) Chordwise static surface pressure distribution (b) Spanwise static surface pressure distribution

Figure 14. Effect of blended winglet on the wing static surface pressure distribution, $\alpha = 10$.

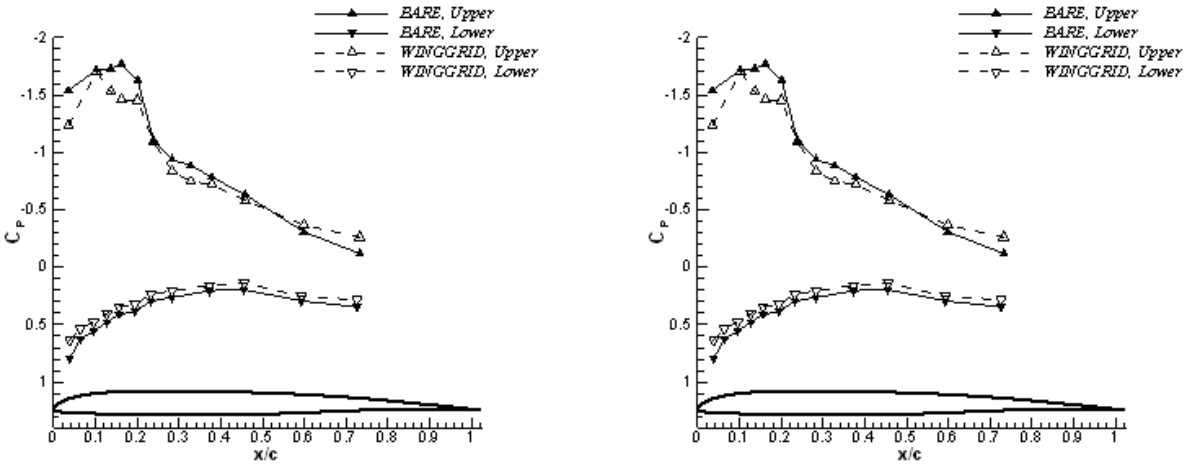

(a) Chordwise static surface pressure distribution (b) Spanwise static surface pressure distribution

Figure 15. Effect of winggrid on the wing surface pressure distribution, $\alpha = 10^{\circ}$.

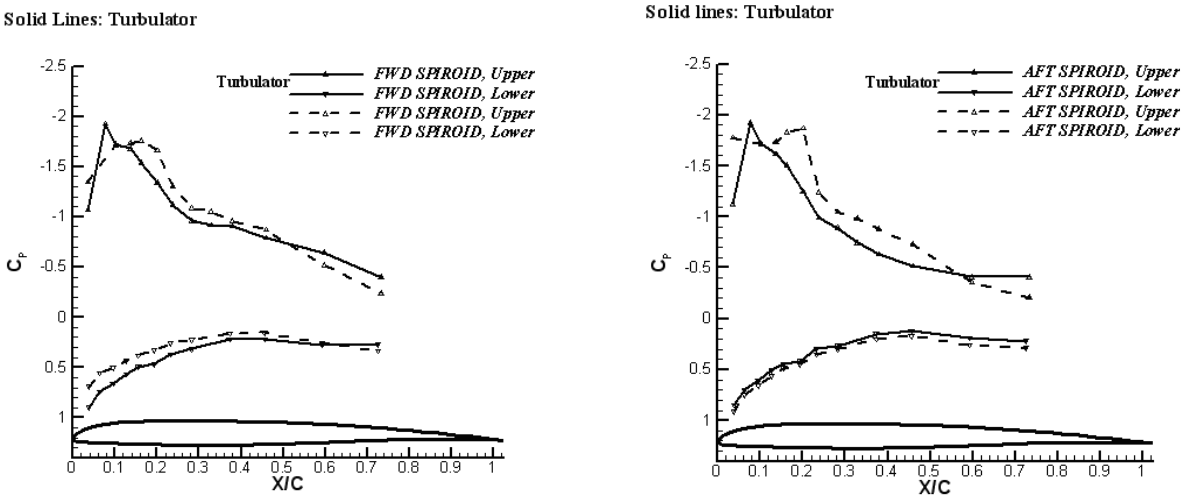

(a) FWD spiroid (b) AFT spiroid

Figure 16. Effect of turbulator strip on the wing chordwise static surface pressure distribution, $\alpha = 10^{\circ}$.

plastic adhesive. The turbulator tape is applied at 10% average chord from the wing leading edge.

Figure 16 shows a comparison between the chordwise static pressure distribution on FWD and AFT spiroid winglets with and without the turbulator strip. It is clearly seen that according to reference [36], with the selected sandpaper, the flow past the turbulator strip is most probably turbulent [37] and the adverse pressure gradient increases drastically with a steeper slope when the wing is equipped with the turbulator located.

Further, Figure 16a shows that the turbulator has changed the pressure distribution on both upper and lower surfaces. It seems that the transition over the model upper surface is likely to occur at x/c≈0.1. For the lower surface the upper turbulator increases only the pressure distribution along the chord resulting in higher lift. It should be noted that for the clean model the absolute value of pressure coefficient over the upper surface increases from x/c=0.04 to its maximum value at x/c=0.12. For the range of x/c=0.12 to x/c=0.20, C_P on the upper surface remains nearly constant. For x/c≥0.20, the magnitude of C_P on the model upper surface starts to decrease, indicating pressure recovery. However, when the turbulator strip is added to the model, the constant pressure region seen for the clean model vanishes. Instead, a sharp pressure rise is generated followed by a steep pressure recovery region in the vicinity of the model leading edge. For the AFT spiroid case, Figure 16b, the scenario is slightly different from that of the FWD one, Figure 16a. Here, the pressure distribution over the clean model remains nearly constant for 0.02≤x/c≤0.20 and then increases sharply for higher x/c. Similarly, an addition of the turbulator strip leads to a variation of the upper surface pressure distribution in the vicinity of the model leading edge drastically as seen from Figure 16b. However, no significant changes are observed in the C_P distribution for the lower surface. For the AFT spiroid case, the turbulator strip reduces the overall sectional lift coefficient (Figure 16b) while for the FWD one, no significant changes in the overall sectional lift coefficient is observed (Figure 16a).

Total Pressure Distribution

In order to measure the total pressure distribution behind the wing, a 32-tube rake probe was mounted horizontally at the back of the model. The measurement nodes comprised of approximately 2500 points which form a grid as shown in Figure 7. Note that the total pressure distribution is measured in the wake of the model at a distance of x/c=2 which was selected after considerable measurements at different positions behind the wing. Total pressure measurements were conducted for four different winglet configurations introduced in the preceding sections, including bare wing for comparison, at different angles of attack.

Figure 17 a-e shows total pressure distribution behind the wing with four different winglets at zero angle of attack. It can be seen by inspection that at zero angle of attack, the tip vortex for the bare wing is quite clear. The airfoil used in this wing is not symmetric; thus, at zero angle of attack, some lift is generated as a result of different pressure distributions over its upper and lower surfaces. Hence, a tip vortex is further generated as seen in Figure 17a. Furthermore, the tip vortices for the cases with winglets are different from those for the bare wing (Figure 17b-e). It can be seen by inspection that the tip vortex for the blended winglet (Figure 17b), is weaker than the other ones. For other winglets, FWD spiroid, AFT spiroid, and the winggrid, the shape and width of the tip vortex differ significantly from those of the bare and blended ones.

The effects of angle of attack on the tip vortices formed by those winglets are also shown in Figures 18 and 19. Similar, the data for the bare wing are shown for both angles of attack (α=10, 15°) for comparison. It is shown that as the angle of attack increases, the height, width, and strength of the tip vortices varies significantly. The tip vortex for the clean model moves inward (toward the root) and the vortex core widens (Figures 18a and 19a).

Figure 18a shows that the maximum height of the tip vortex core for the clean model at α=10° is about ζ≈-0.02, while for the other two cases, as shown in Figures 17a and 19a, it is ζ=0.05 and ζ=-0.03.

A comparison of Figures 18c and 18d reveals that the FWD spiroid winglet displaces the wake upward, i.e. above the primary tip vortex, while the AFT spiroid case moves the wake below the primary tip vortex. The wake formation behind these two winglets, FWD spiroid and the AFT as seen from Figure 18, differs from each other significantly. More detailed experiments are suggested to better understand these phenomena. The effect of blended winglet on the total pressure distribution in the wake of the model measured at x/c=2.0 and α=10° is shown in Figure 18b. From this figure, two relatively weak tip vortices are identified. The total pressure loss caused by these vortices in the wake of the model is less than that of the bare wing (Figure 18a). Furthermore, comparing Figures 18a and 18b, it can be seen that the height of the tip vortex of the bare wing is much lower than that of the blended one. The blended winglet creates two tip vortices, one reaches a maximum height of about ζ=0.05 and the second reaches ζ=0.45; however, the maximum height of the core of the tip vortex for the bare wing is ζ=-0.02 (Figure 18a). Furthermore, it should be mentioned that the first tip vortex of the blended winglet is much weaker than that of the

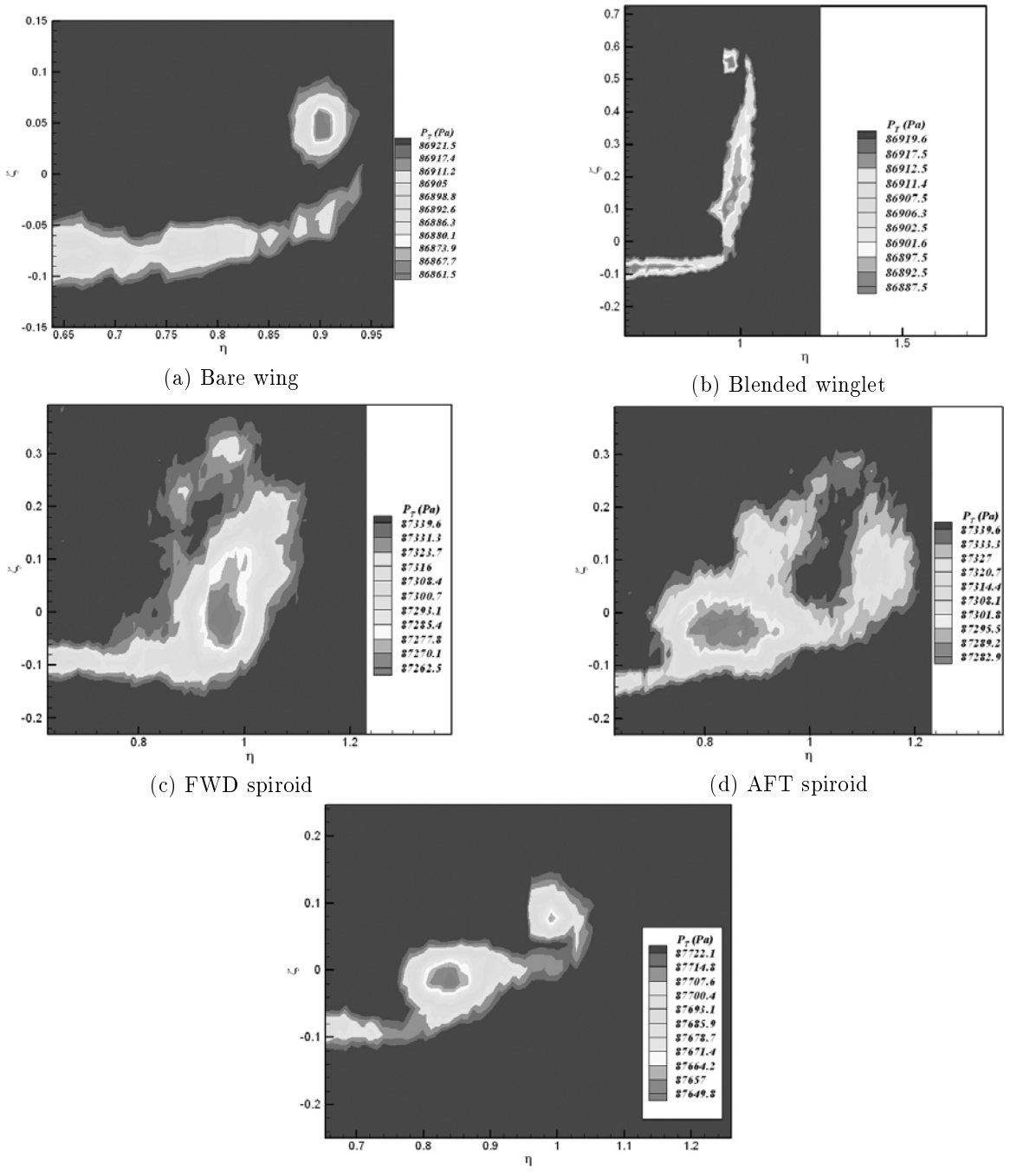

Figure 17. Effect of different winglet shapes on total pressure distribution behind the wing, $\alpha = 0^{\circ}$.

bare wing. Comparing Figure 18a and 18b, one may conclude that the primary tip vortices have almost the same height, $\zeta \approx 0$, although the blended winglet has displaced the primary tip vortex slightly upward, $\zeta \approx 0.025$. However, the blended winglet has created another vortex which is located at a height of about $\zeta = 0.45$. This vortex is believed to be due to the blended winglet itself which acts as a half model wing attached at one end to the primary model tip instead of the tunnel wall. Thus, this winglet might generate a tip vortex when the flow passes over it. However, for the spiroid cases shown in Figure 18, the situation is different. In addition, it should be noted that both ζ and η for the tip vortex of the bare wing are much larger than those of the blended winglet ones, i.e. the bare wing has a much larger tip

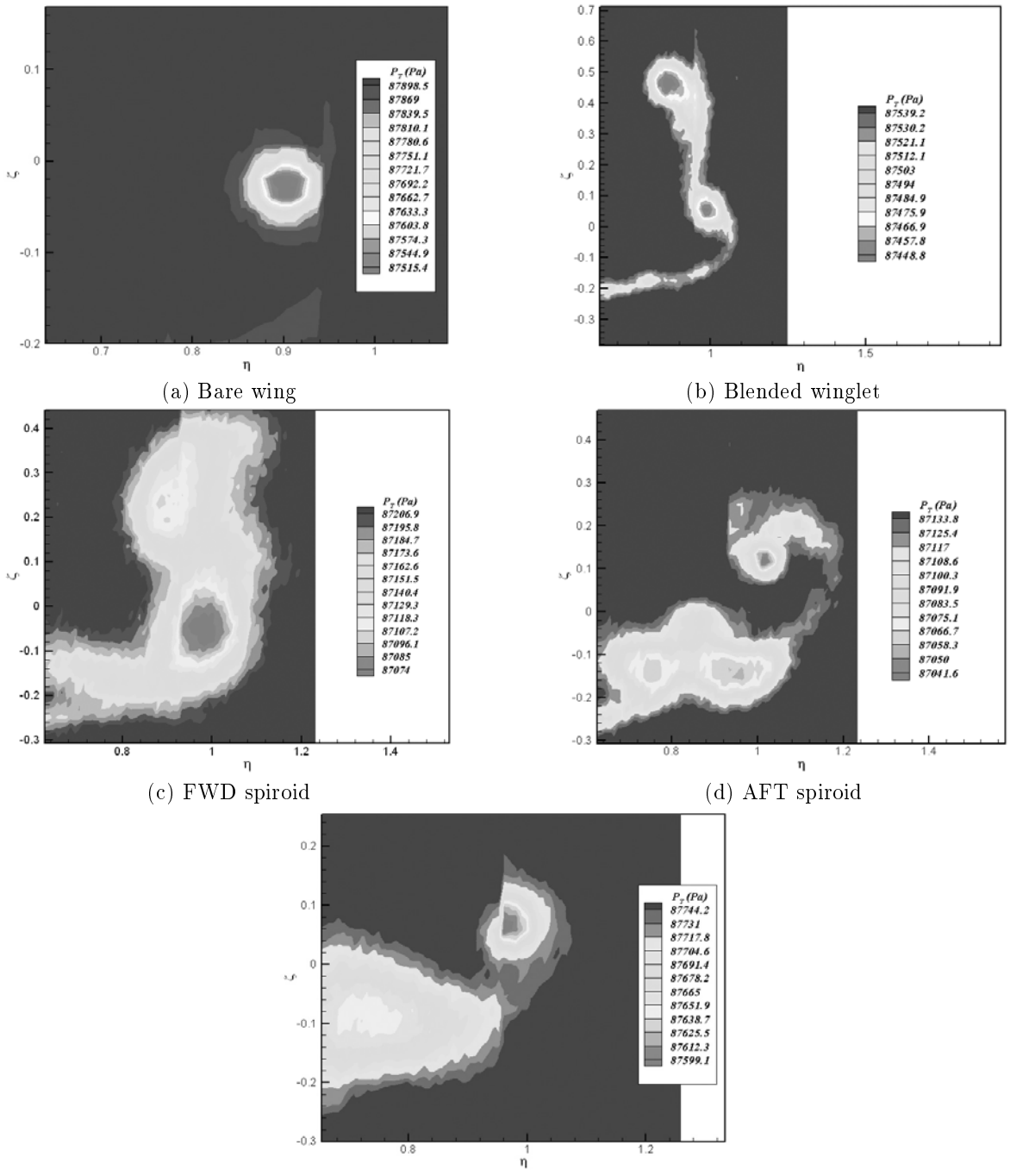

Figure 18. Effect of different winglet shapes on total pressure distribution behind the wing, $\alpha = 10^{\circ}$.

vortex. Moreover, a comparison of Figures 18c and 18d with Figure 18b indicates that the width of the wake generated by the blended winglet is much smaller than those of the spiroid ones. It should be emphasized that all cases shown here are for the same angle of attack and the measured total pressure are at the same distance behind the model, x/c=2.0. Figure 18e shows total wake pressure distribution at x/c=2.0 behind the model equipped with the winggrid. Although the tip vortex formed by this winglet is similar to that of the bare wing one, Figure 18a, the wake behind the model is different. Further it seems that this type of winglet has displaced the tip vortex too, $\zeta \approx 0.05$. Note that for the bare wing case, under the same conditions, the height of the vortex core was about $\zeta \approx -0.025$. Other

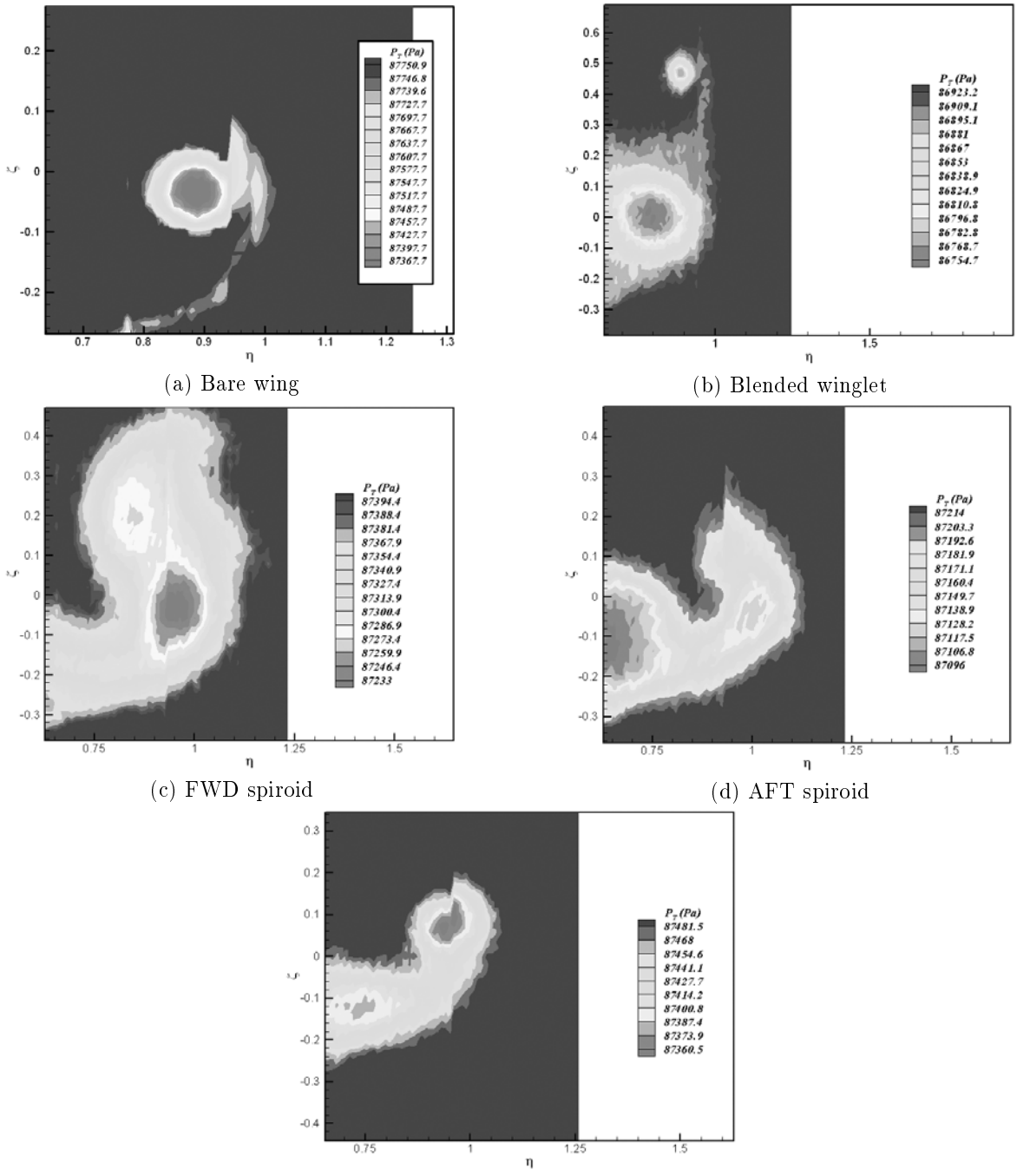

(a) Bare wing

(b) Blended winglet

(c) FWD spiroid

(d) AFT spiroid

(e) Wing grid

Figure 19. Effect of different winglet shapes on total pressure distribution behind the wing, $\alpha = 15^{\circ}$.

data at different angles of attack show similar trends [38, 39].

For higher angle of attack (α=15°) (Figure 19), the shape of vortices formed behind the wing equipped with winglets vary significantly with those at lower alpha (Figure 18). Here, the main vortex formed by the blended winglet is widened and has moved inward, Figure 19b. However, the second vortex formed by this winglet, due to the winglet itself is much weaker than that of Figure 18b. Furthermore, Figures 18c and 19c illustrate that the changes in the tip vortex of the FWD spiroid are much less than those of the AFT one (Figures 18d and 19d). Finally, the flowfield behind the wing equipped with winggrid also shows some variations with the angle of attack. As alpha increases, the tip vortex is moved toward the wing root

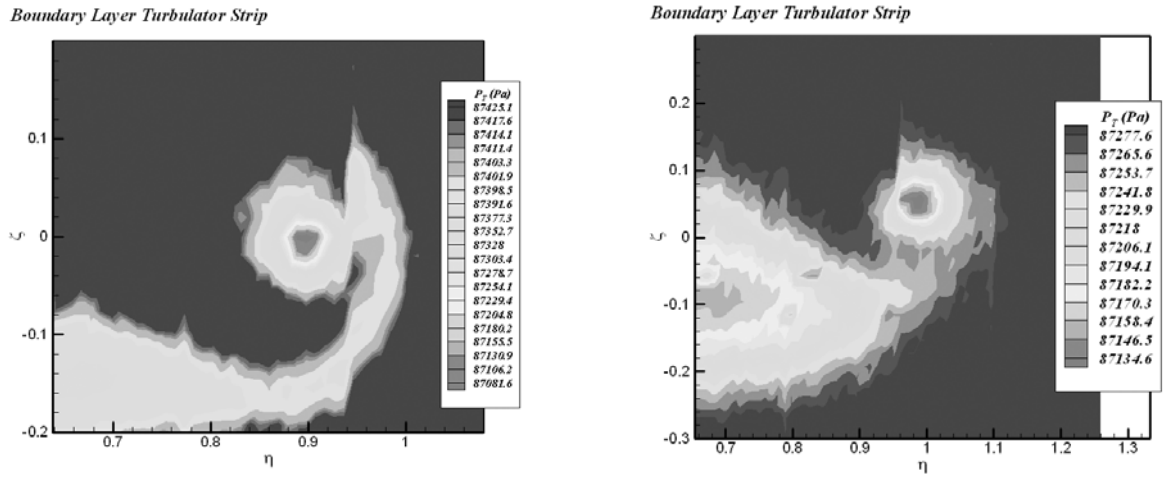

(a) Bare wing (b) Wing grid

Figure 20. Effect of turbulator strip on the wing total pressure distribution, α=10°.

and is shifted downward slightly (Figures 18e and 19e). Similar trends are also observed for other angles of attack, α=-10 to 15 degrees, reference [38, 39].

Total Surface Pressure Distribution with Turbulator Tape

Figure 20 shows variations of the total pressure behind the bare wing and wing with winggrid at $\alpha = 10°$. For both cases, the model is equipped with turbulator strip installed at x/c=0.1; hence, creating early flow transition. Comparing the total pressure distribution behind the wing for this case with those without turbulator (Figures 18a and 18e), it can be seen that the turbulator has not changed the shape and orientation of the vortices significantly. However, the wake behind the model with turbulator is slightly thickened and the total pressure has been reduced, Figure 20. Surface pressure data [38] shows similar trend and indicates that the transition occurs at a place where the turbulator is installed. The total pressure reduction is due to the change of the laminar flow to turbulent while the difference in the flow regime has only quantitative effect.

CONCLUSION

An extensive experimental investigation is conducted to study the effect of different winglet shapes on a tapered wing surface pressure distribution, chordwise and spanwise, as well as the total pressure in the wake. Four different winglet shapes are used for this study. The effect of Reynolds number was investigated by forcing early transition over the model surface at about x/c $\approx$ 0.1.

While the surface pressure results do not show significant effects, roughness seems to move the transition point forward. The total pressure data in the wake illustrates significant changes for different winglets but at the same angle of attack. The tip vortices formed by different winglet shapes are totally different from each other and indicate a significant effect on the flowfield over the wing surface. These vortices vary differently while the model angle of attack changes. The value of the total pressure measured behind these winglets differs from each other as well, indicating their effect on the induced drag. Furthermore, it is observed that winglets displace the primary tip vortex and change sharp comparing to the bare model. However, these variations differ from one winglet to another.

The results also indicate that for all winglets examined in this study, the total pressure loss in the wake is less than that of the bare wing. However, the winggrid type does not have a significant effect on either the wake data or the surface pressure one. Further, different winglet shapes modified the surface pressure data when the wing angle of attack is ten degrees or higher. The wake behind the wing is drastically changed when the model is equipped with different winglets. More experiments are needed to further examine this statement. Finally, based on the results presented in this paper, FWD Spiroid winglet seems to be more suitable for the cruise flight phase (as the angle of attack is low), whereas the AFT Spiroid winglet is more suitable for the climb phase where the angle of attack is higher than that of the cruise.

ACKNOWLEDGMENT

The present work has been funded in part by the Institute for Aeronautical Research, Bureau of Aircraft Design, HESA. The authors would like to express their appreciation to the Director of the Design Bureau for his support.

REFERENCES

1. Bourdin, P., "Plan form Effects on Lift-induced Drag", *AIAA-2002-3151*, 20th AIAA Applied Aerodynamics Conference, St. Louis, Missouri, (2002).
2. Gold, N. and Visser, K.D., "Aerodynamic Effects of Local Dihedral on a Raked Wingtip", *AIAA-2002-0831*, 40th Aerospace Sciences Meeting & Exhibit, Reno, NV, (2002).
3. Whitcomb, R.TA., "Design Approach and Selected Wind Tunnel Results at High Subsonic Speeds for Wing-Tip Mounted Winglet", *NASA TN-D-8260*, NASA Langley Res. Center, Hampton, VA, (1976).
4. Whitcomb, RT., "Research on methods for reducing the aerodynamic drag at transonic speeds", *The Inaugural Eastman Jacobs Lecture*, NASA Langley Res. Center, Hampton, VA, (1994).
5. Reid, EG., "The effects of shielding the tips of airfoils", *NACA Rep. 201*, Natl. Advis. Comm. Aeronaut., Hampton, VA, (1924).
6. Hemke, PE., "Drag of Wings with Endplates", *NACA Rep. 267*, Natl. Advis. Comm. Aeronaut., Hampton, VA, (1927).
7. Mangler, W., "The lift distribution of wings with end plates", *NACA TM 856*, Natl. Advis. Comm. Aeronaut., Hampton, VA, (1938).
8. Kroo, I., "DRAG DUE TO LIFT, Concepts for Prediction and Reduction", *Annu. Rev. Fluid Mech*, **33**, PP 587-617(2001).
9. Yates, John E., and Donaldson, Coleman duP., "Fundamental Study of Drag and an Assessment of Conventional Drag-Due-To-Lift Reduction Devices", *NASA Contract Rep 4004*, Langley Res. Center, Hampton, VA, (1986).
10. Thiede, P., "Aerodynamic Drag Reduction Technologies", Proceedings of the CEAS/DragNet European Drag Reduction Conference, 19-21, June 2000, Potsdam, Germany, 1^{st} Ed., (2001).
11. Patterson, J.C., "Wingtip Vortex Turbine", *United States Patent # 4*, (1991).
12. Abeyounis, William, K., H. Paul, Stough, III, Lt., Col., Alfred, J., Wunschel and Patrick, D., Curran, "Wingtip Vortex Turbine Investigation for Vortex Energy Recovery", *SAE AEROTECH '90 (901936)*, SAE Aerospace Technology Conference & Exposition, (1990).
13. Janus, J., Mark, Animesh Chatterjee and Chris, Cave, "Computational Analysis of a Wingtip-Mounted Pusher Turboprop", *Journal of Aircraft*, **33(2)**, (1995).
14. Eppler, R., "Induced Drag and Winglets", *Aerospace Science and Technology*, PP 3-15(1997).
15. Vijgen, P. M. H. W., van Dam, C. P., and Holmes, B. J., "Sheared Wing-Tip Aerodynamics: Wind-Tunnel and Computational Investigation", *Journal of Aircraft*, **26(3)**, PP 207(1989).
16. Gall, P. D. and Smith, H. C., "Aerodynamic Characteristics of Biplanes with Winglets", *AIAA J. Aircraft*, **24(8)**, PP 518(1987).
17. Mann, A. and Elsholz, I. E., "The M-DAW Project: Investigations in Novel Wing Tip Device Design", *AIAA-2005-0461*, 43^{rd} Aerospace Sciences Meeting & Exhibit, Reno, NV, (2005).
18. Ogurek, D. J. and Ashworth, J., "Experimental Investigation of Various Winglet Designs for a Wing in Ground Effect", *AIAA-2004-4720*, 22^{nd} Applied Aerodynamics Conference and Exhibit, Providence, Rhode Island, (2004).
19. La Roche, U. and La Roche, H. L., "Induced Drag Reduction using Multiple Winglets, looking beyond the Prandtl-Munk Linear Model", *AIAA 2004-2120*, 2^{nd} AIAA Flow Control Conference, Portland, Oregon, (2004).
20. Smith, M. J. et al., "Performance Analysis of a Wing with Multiple Winglets", *AIAA-2001-2407*, 19^{th} AIAA Applied Aerodynamics Conference, Anaheim, CA, (2001).
21. Smith, L. A. and Campbell, R. L., "Effects of Winglets on the Drag of a Low-Aspect-Ratio Configuration", *NASA Technical Paper 3563*, Langley Research Center, Hampton, VA, (1996).
22. Flechner, S. G., Jacobs, P. F., and Whitcomb, T., "A High Subsonic Speed Wind-Tunnel Investigation Of Winglets On A Representative Second-Generation Jet Transport Wing", *NASA TN D-8264*, NASA Langley Research Center, Hampton, VA, (1976).
23. Asai, K., "Theoretical Considerations in the Aerodynamic Effectiveness of Winglets", *Journal of Aircraft*, **22(7)**, PP 635(1985).
24. Park, P. S. and Rokhsaz, K., "Effects of a Winglet Rudder on Lift-to-Drag Ratio and Wake Vortex Frequency", *AIAA 2003-4069*, 21^{st} Applied Aerodynamics Conference, Orlando, Florida, (2003).
25. Reneaux, J., "Overview on Drag Reduction Technologies for Civil Transport Aircraft", European Congress on Computational Methods in Applied Sciences and Engineering, ECCOMAS, Jyvaskyla, (2004).
26. Grenon, R. and Bourdin, P., "Numerical Study of Unconventional Wing Tip Devices for Lift-Induced Drag Reduction", CEAS Aerospace Aerodynamics Research Conference, (2002).
27. Soltani, M. R., and Davari, A. R., "An Experimental Investigation of the Flowfield over a Low Aspect Ratio Wing", *Esteghlal Journal of Engineering*, Isfahan University of Technology, **20(2)**, (2002).
28. Soltani, M. R., T. Khadivi and A. Abbasi Hoseini, "Flow Field Study Over the Wing of a Fighter-Type Aircraft Model", *International Journal of Engineering*, Transaction B: Applications, **17(4)**, PP 405-416(2004).
29. Gratzer, Louis, B., "Spiroid-Tipped Wing", *United States Patent # 5*, 102,068, (1992).

30. Gratzer, Louis, B., "Blended Winglet", *United States Patent # 5*, 348, 253, (1994).
31. La Roche, "Wing with a Wing Grid as the End Section", *United States Patent # 5*, 823, 480, (1998).
32. La Roche et al., "Wing Comprising a Distal Wing Grid", *United States Patent # 6*, 431, 499, B1, (2002).
33. Hurt, H. H., Jr., "Aerodynamics for Naval Aviators", The office of the chief of naval operations, Aviation Training Division, U.S. Navy, (1965).
34. Liu, M.J. et al., "Flow Patterns and Aerodynamic Characteristics of a Wing-Strake Configuration", *AIAA J. of Aircraft*, Article No. 79-1877R, **17**(5), (1980).
35. Albert E. von Doenhoff; Elmer A. Horton, "A Low-Speed Experimental Investigation of the Effect of a Sandpaper Type of Roughness on Boundary-Layer Transition", *NACA Report 1349*, (Supersedes NACA Technical Note 3858), (1956).
36. Rae H., William Jr., Allan Pope, *Low-Speed Wind Tunnel Testing*, 2nd Ed., John Wiley & Sons, (1984).
37. Soltani M.R., Ghorbanian K. and Nazarinia M., "Flow Analysis Over and Behind a Wing with Different Winglet Shapes", *AIAA 2004-0723*, 42^{nd} Aerospace Sciences Meeting & Exhibit, Reno, NV, (2004).
38. Soltani M.R., Ghorbanian K. and Nazarinia M., "Experimental Investigation of the Effect of Various Winglet Shapes on the Total Pressure Distribution behind a Wing", 24^{th} ICAS Congress, Yokohama, Japan, (2004).